JOURNAL OF MATERIALS PROCESSING TECHNOLOGY 209 (2009) 847–855

journal homepage: www.elsevier.com/locate/jmatprotec

A novel hob cutter design for the manufacture of spur-typed cutters

Jen-Kuei Hsieh[a], *Huang-Chi Tseng*[b], *Shinn-Liang Chang*[b,*]

[a] *Mechanical Engineering Department, National Chiao Tung University, EE507, 1001 Ta Hsueh Road, Hsinchu 30010, Taiwan, ROC*
[b] *Institute of Mechanical and Electro-Mechanical Engineering, National Formosa University, Huwei Township, Yunlin County, Taiwan, ROC*

ARTICLE INFO

Article history:
Received 23 November 2007
Received in revised form
20 February 2008
Accepted 24 February 2008

Keywords:
Hob cutter
Spur-typed cutter
Undercutting

ABSTRACT

Spur-typed cutters with multiple cutting angles are important tools frequently used in the manufacture of many machine elements. Due to their complex geometry, the production of these cutters involves milling and several grinding processes. Such a complex manufacturing process, coupled with the need for expensive manufacturing tools, makes the cutters costly.

Undercutting is a phenomenon that causes weakness at the root of a gear. Engineers use shifted gears, modified tooth profiles, or changes in the pressure angle to overcome undercutting in gears. However, in this paper, by utilizing the undercutting phenomenon, a novel design of straight-sided hob cutter with multiple pressure angles is proposed for the manufacture of spur-typed cutters. With the simultaneous application of multiple pressure angles, this tool design concept significantly simplifies the manufacturing process. The effects of cutting angles, the degree of undercutting, and the width of the top land of the cutter are studied. The concepts and results proposed in this paper are beneficial as design guidance for tool designers and manufacturers.

1. Introduction

Spur-typed cutter, which is formed with multiple cutting angles, is one of the most frequently used tools in the manufacture of machine components. The production of these cutters involves milling, rough grinding, and finish grinding. Due to the complex geometry and manufacturing process, various expensive manufacturing tools must be employed, and hence the manufacture of the cutters can be very costly.

The hobbing of gears is the most effective manufacturing process found in the gear industry. New suggestions and methods to improve the precision and efficiency of hobbing have been introduced by researchers. Cluff (1987) investigated how the generating accuracy of hob cutter was affected by cutter geometric peculiarities and resharpening errors. Radhakrishnan et al. (1982) proposed a method to obtain the grinding wheel profile of the twist drill flute in resharpening. Ainoura and Nagano (1987) investigated the conventional hobbing using a hob with its helix running in the direction opposite the gear, and they found it more effective for the high-speed manufacture of comparatively small module gears for automobiles. In Koelsch's research (1994), hobbing cutters with different coatings are tested in high-speed cutting, and cermets were found to posses the best performance in high-speed dry cutting. More specifically, Phillips (1994) indicated that hob cutter coated by titanium nitride made productivity

* *Corresponding author at*: Room 529, Building 2, The New Campus, National Formosa University, No. 64, Wunhua Road, Huwei Township, Yunlin County 632, Taiwan, ROC. Tel.: +886 5 6315429; fax: +886 5 6312110.
E-mail address: changsl@nfu.edu.tw (S.-L. Chang).
0924-0136/$ – see front matter © 2008 Elsevier B.V. All rights reserved.
doi:10.1016/j.jmatprotec.2008.02.071

realized. Bouzakis and Antonidais (1995) proposed a computational procedure, which enables the determination of optimum values for the shift displacement and for the corresponding shift amount.

In theory, the hob cutter may be considered to be a worm that is slotted in the axial direction to form a series of cutting blades. In Litvin's publication (1989), the axial section of the worm was considered as the rack. Most of the literature uses rack cutters to simulate the generating process of a hob cutter. Tsay (1988) investigated helical gears with involute shaped teeth, whose mathematical description was derived by straight-sided rack cutter. Chang et al. (1997a) proposed a general mathematical model of gear generated by CNC hobbing machine. Recent research, relevant to the hobbing process, includes the paper of Chang et al. (1996), in which the manufacture of elliptical gears was studied. Chang (1996) simulated the hobbing process through a computer numerically controlled (CNC) hobbing machine. Chang et al. (1997b) achieved design optimization by tuning parameters of modified helical gear train. More recently, Kapelevich (2000) investigated the hobbing of an unsymmetrical involute tooth profile. Chang et al. (2002) patented a new hob cutter profile that generated a helical cutting tool. The mathematical model of this helical cutting tool is presented in the paper written by Liu and Chang (2003). However, the above-published work presented little systematic and in-depth discussion on the design and generation of the cutting tool tooth profile. In particular, there were no discussions of the design of a hob cutter capable of generating a spur-typed cutter with multi-cutting angles. Therefore, the possibilities for modifying existing designs are limited.

Undercutting is a phenomenon that causes weakness at the root of a gear. Various methods have been used to overcome this problem. In this paper, a novel design for a straight-sided hob cutter with multiple pressure angles is proposed, and the undercutting phenomenon is used to facilitate the manufacture spur-typed cutters. The proposed hob cutter can generate the multiple cutting angles simultaneously, which significantly reduces time and cost required in the traditional process. The multiple pressure angles of hob cutter include a large pressure angle that generates the involute surface of the spur-typed cutter, which acts as the main body. A smaller pressure angle of, possibly, less than 5°, undercuts the spur-typed cutter and forms the radial rake angle, which is a special application of undercutting in gear geometry. A third pressure angle, which is the largest one in the hob cutter, generates the relief and clearance angles. Characteristics of the spur-typed cutter, including cutting angles, top land width, and full undercutting, are all studied.

The main theme of this paper is the concept of using multiple pressure angles to generate the complex multiple cutting angles. The developed mathematical model and the conducted analyses contribute a lot both in designing and manufacturing the spur-typed cutters.

2. A novel design for a hob cutter

A hob cutter with straight-sided cutting face is commonly used in the manufacture of involute gear. An improper parameter design of the cutter will cause the undercutting at the roots of the gear. However, by appropriately designing the parameters of hob cutter, the undercutting can be controlled and become beneficial. Fig. 1 shows the normal section of the novel type hob cutter, which is also considered as the profile of a rack cutter. The cutting face of Fig. 1 can be divided into six regions, i.e. left cutting face I, right cutting face II, fillet cutting faces III and IV, top land cutting face V, and chamfering cutting face VI. The profile is almost similar to an ordinary hob cutter for involute gears, except for the two large pressure angles, i.e. regions I and VI, and a small pressure angle, i.e., region II. The cutting face II, with its small pressure angle, generates the cutting face and radial rake angle of the cutter by undercutting. The cutting face I, with its large pressure angle, generates the main body of the cutter. The cutting face VI, with the largest pressure angle, generates the clearance and relief angles of the cutter. The origin of the coordinate system $\mathbf{S}_a(X_a, Y_a, Z_a)$ is located at the middle of the rack cutter body. The positive X_a axis is set upwards; positive Y_a is directed to the right, while the Z_a axis can be determined by the right-hand rule. In Fig. 1, ξ represents the pitch line of the rack cutter, ψ_L is the pressure angle of the left straight-sided cutting face, ψ_R is the pressure angle of the right straight-sided cutting face, and ψ_3 is the largest pressure angle cutting face VI. HKW is the addendum of the rack cutter and HFW is the dedendum of the rack cutter, while $2b_0$ and P_0 represent the tooth thickness and pitch of the rack cutter, respectively. In this paper, the theory of gearing proposed by Litvin (1989), which considers the locus equation and meshing equation simultaneously, is used to generate the tooth profile of the cutter.

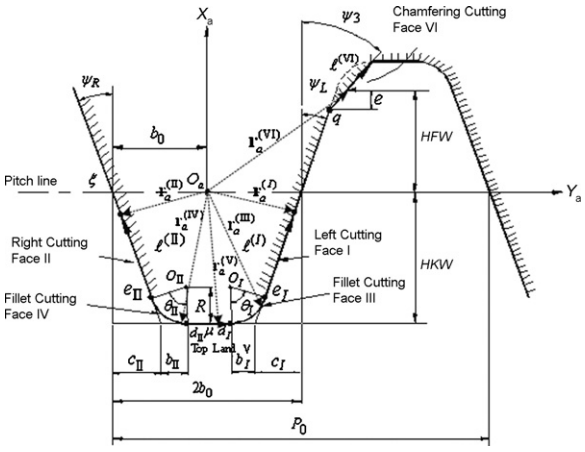

Fig. 1 – Normal section of hob cutter.

2.1. *Equations for the rack cutter*

The equations for the six regions of the cutting face shown in the $\mathbf{S}_a$ coordinate system can be represented as follows:

(1) Left cutting face I:
The coordinates of the origin point e_I of the cutting face I in Fig. 1 can be shown as

$$x_a^{(e_I)} = R - HKW - R\sin\psi_L \quad (1)$$

$$y_a^{(e_I)} = b_0 - \frac{R}{\tan(45+\psi_L/2)} - HKW\tan\psi_L + R\cos\psi_L \quad (2)$$

When parameter $\ell^{(I)}$ indicates the position on the cutting face I, the equation of this cutting face can thus be represented in the $\mathbf{S}_a$ coordinate system as the following equation:

$$r_a^{(I)} = \begin{bmatrix} R - HKW - R\sin\psi_L + \ell^{(I)}\cos\psi_L \\ b_0 - \dfrac{R}{\tan(45+\psi_L/2)} - HKW\tan\psi_L + R\cos\psi_L + \ell^{(I)}\sin\psi_L \\ 0 \\ 1 \end{bmatrix} \quad (3)$$

The unit normal to this cutting face is obtained as

$$\mathbf{n}_a^{(I)} = \sin\psi_L\mathbf{i}_a - \cos\psi_L\mathbf{j}_a \quad (4)$$

(2) Right cutting face II:
The coordinates of the origin point e_{II} of the cutting face II in Fig. 1 can be shown as

$$x_a^{(e_{II})} = R - HKW - R\sin\psi_R \quad (5)$$

$$y_a^{(e_{II})} = -b_0 + \frac{R}{\tan(45+\psi_R/2)} + HKW\tan\psi_R - R\cos\psi_R \quad (6)$$

When parameter $\ell^{(II)}$ indicates the position on the cutting face II, the equation of this cutting face can thus be represented in the $\mathbf{S}_a$ coordinate system as

$$\mathbf{r}_a^{(II)} = \begin{bmatrix} R - HKW - R\sin\psi_R + \ell^{(II)}\cos\psi_R \\ -b_0 + \dfrac{R}{\tan(45+\psi_R/2)} \\ +HKW\tan\psi_R - R\cos\psi_R - \ell^{(II)}\sin\psi_R \\ 0 \\ 1 \end{bmatrix} \quad (7)$$

The unit normal to this cutting face is obtained as

$$\mathbf{n}_a^{(II)} = -\sin\psi_R\mathbf{i}_a - \cos\psi_R\mathbf{j}_a \quad (8)$$

(3) Fillet cutting face III:
In Fig. 1, parameter R is the radius of fillet. The geometry shows that $C_I = HWK\tan\psi_L$ and $b_I = R/\tan(45+\psi_L/2)$. Coordinates of the origin O_I of the fillet cutting face III can be shown as

$$x_a^{(O_I)} = R - HKW \quad (9)$$

$$y_a^{(O_I)} = b_0 - \frac{R}{\tan(45+\psi_L/2)} - HKW\tan\psi_L \quad (10)$$

Parameter θ_I indicates the position on the fillet cutting face III, which defines the cutting face position with the X_a axis for $0 \le \theta_I \le (90-\psi_L)$. The equation of this cutting face can thus be represented in the $\mathbf{S}_a$ coordinate system as the following equation:

$$r_a^{(III)} = \begin{bmatrix} R - HKW - R\cos\theta_I) \\ b_0 - \dfrac{R}{\tan(45+\psi_L/2)} - HKW\tan\psi_L + R\sin\theta_I \\ 0 \\ 1 \end{bmatrix} \quad (11)$$

The unit normal to this cutting face is obtained as

$$\mathbf{n}_a^{(III)} = \cos\theta_I\mathbf{i}_a - \sin\theta_I\mathbf{j}_a \quad (12)$$

(4) Fillet cutting face IV:
If parameter R defines the radius of the fillet, Fig. 1 shows that $C_{II} = HKW\tan\psi_R$ and $b_{II} = R/\tan(45+\psi_R/2)$. Coordinates of the origin O_{II} of the fillet cutting face IV can be shown as

$$x_a^{(O_{II})} = R - HKW \quad (13)$$

$$y_a^{(O_{II})} = -b_0 + \frac{R}{\tan(45+\psi_R/2)} + HKW\tan\psi_R \quad (14)$$

Parameter θ_{II} indicates the position on the fillet cutting face III, which defines the cutting face position with the X_a axis for $0 \le \theta_{II} \le (90-\psi_R)$. The equation of this cutting face can thus be represented in the $\mathbf{S}_a$ coordinate system as

$$\mathbf{r}_a^{(IV)} = \begin{bmatrix} R - HKW - R\cos\theta_{II} \\ -b_0 + \dfrac{R}{\tan(45+\psi_R/2)} + HKW\tan\psi_R - R\sin\theta_{II} \\ 0 \\ 1 \end{bmatrix} \quad (15)$$

The unit normal of this cutting face is obtained as

$$\mathbf{n}_a^{(IV)} = -\cos\theta_{II}\mathbf{i}_a - \sin\theta_{II}\mathbf{j}_a \quad (16)$$

(5) Top land cutting face V:
The top land cutting face V is formed by two tangential points d_{II} and d_I. The coordinates of point d_{II} in the $\mathbf{S}_a$ coordinate system are

$$x_a^{(d_{II})} = -HKW \quad (17)$$

$$y_a^{(d_{II})} = -b_0 + \frac{R}{\tan(45+\psi_R/2)} + HKW\tan\psi_R \quad (18)$$

And the coordinates of point d_I in the $\mathbf{S}_a$ coordinate system are

$$x_a^{(d_I)} = -HKW \quad (19)$$

$$y_a^{(d_I)} = b_0 - \frac{R}{\tan(45+\psi_L/2)} - HKW\tan\psi_L \quad (20)$$

Parameter μ indicates the position of point d_{II} along the Y_a direction and $0 \le \mu \le (Y_a^{d_I} - Y_a^{d_{II}})$. The equation of this cutting face can thus be represented in the $\mathbf{S}_a$ coordinate

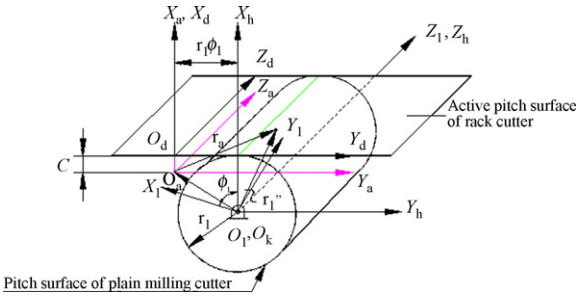

Fig. 2 – Coordinate system relationship of rack cutter and generated gear.

system as the following equation:

$$\mathbf{r}_a^{(V)} = \begin{bmatrix} -\mathrm{HKW} \\ -b_0 + \dfrac{R}{\tan(45+\psi_R/2)} + \mathrm{HKW}\tan\psi_R + \mu \\ 0 \\ 1 \end{bmatrix} \quad (21)$$

The unit normal of this cutting face is obtained as

$$\mathbf{n}_a^{(V)} = \mathbf{i}_a \quad (22)$$

(6) Chamfering cutting face VI:
The coordinates of the starting point q on this cutting face in Fig. 1 can be shown as

$$x_a^{(q)} = \mathrm{HFW} - e \quad (23)$$

$$y_a^{(q)} = b_0 + (\mathrm{HFW} - e)\tan\psi_L \quad (24)$$

Parameter $\ell^{(VI)}$ indicates the position on the cutting face VI. The equation of this cutting face can thus be represented in the $\mathbf{S}_a$ coordinate system as the following equation:

$$\mathbf{r}_a^{(VI)} = \begin{bmatrix} \mathrm{HFW} - e + \ell^{(VI)}\cos\psi_3 \\ b_0 + (\mathrm{HFW} - e)\tan\psi_L + \ell^{(VI)}\sin\psi_3 \\ 0 \\ 1 \end{bmatrix} \quad (25)$$

The unit normal to this cutting face is obtained as

$$\mathbf{n}_a^{(VI)} = \sin\psi_3\mathbf{i}_a - \cos\psi_3\mathbf{j}_a \quad (26)$$

2.2. *Locus equations of rack cutter*

When a rack cutter is used to cut gears, the coordinate systems' relationship can be represented as in Fig. 2. In this figure, the theoretical pitch surface of the rack cutter is tangent to the pitch surface of the spur-typed cutter to be cut when the shifted distance C = 0.0. As the theoretical pitch surface of the rack cutter, i.e., the $Y_a - Z_a$ plane, moves toward the spur-typed cutter, C becomes negative. The mathematical model proposed here can then be used to simulate different spur-typed cutters with different shifted distances manufactured by the same rack cutter or hob cutter. In the manufacturing of a spur-typed cutter, the active pitch surface $Y_d - Z_d$ translates towards the left while the generated spur-typed cutter rotates in a counter-clockwise direction. The locus equation of the rack cutter represented in the $\mathbf{S}_1$ coordinate system and attached to the spur-typed cutter represents the cutting process. The generated profile can thus be obtained by solving the locus equation and the meshing equation [(6) and (16)] simultaneously. The meshing equation correlates the surface parameter of the cutting face to the motion parameter of the generation process.

(1) Locus equation of left cutting face I:
The locus equation of the left cutting face I shown in the generated cutter coordinate system $\mathbf{S}_1$ can be obtained by transforming the cutting face equation from $\mathbf{S}_a$ to $\mathbf{S}_1$. The transformation matrix and locus equation are as follow:

$$[\mathbf{M}_{1a}] = \begin{bmatrix} \cos\phi_1 & -\sin\phi_1 & 0 & r_1\phi_1\sin\phi_1 + (r_1 - c)\cos\phi_1 \\ \sin\phi_1 & \cos\phi_1 & 0 & -r_1\phi_1\cos\phi_1 + (r_1 - c)\sin\phi_1 \\ 0 & 0 & 1 & 0 \\ 0 & 0 & 0 & 1 \end{bmatrix} \quad (27)$$

$$\mathbf{r}_1^{(I)} = [\mathbf{M}_{1a}]\cdot\mathbf{r}_a^{(I)} \quad (28)$$

(2) Locus equation of right cutting face II:

$$\mathbf{r}_1^{(II)} = [\mathbf{M}_{1a}]\cdot\mathbf{r}_a^{(II)} \quad (29)$$

(3) Locus equation of fillet cutting face III:

$$\mathbf{r}_1^{(III)} = [\mathbf{M}_{1a}]\cdot\mathbf{r}_a^{(III)} \quad (30)$$

(4) Locus equation of fillet cutting face IV:

$$\mathbf{r}_1^{(IV)} = [\mathbf{M}_{1a}]\cdot\mathbf{r}_a^{(IV)} \quad (31)$$

(5) Locus equation of top land cutting face V:

$$\mathbf{r}_1^{(V)} = [\mathbf{M}_{1a}]\cdot\mathbf{r}_a^{(V)} \quad (32)$$

(6) Locus equation of chamfering cutting face VI:

$$\mathbf{r}_1^{(VI)} = [\mathbf{M}_{1a}]\cdot\mathbf{r}_a^{(VI)} \quad (33)$$

3. Profile of spur-typed cutter

The mathematical model of the generated tooth profile can be obtained by considering the locus equation and the meshing equation [(6) and (16)] simultaneously. The loci equations are shown in the previous section while the meshing equation is represented by the following equation:

$$\mathbf{n}_a^{(n)}\cdot\mathbf{V}^{(12)} = 0 \quad (34)$$

where $\mathbf{n}_a^{(n)}$ is common unit vector normal to the two contact surfaces; $\mathbf{V}^{(12)}$ is the relative velocity between these two contact surfaces.

The meshing equation means that the common normal is perpendicular to the relative velocity at the contact point. It is independent of the selected coordinate system. For convenience, the common unit normal and relative velocity will be represented in the $\mathbf{S}_h$ coordinate system in this paper. From Fig. 2, the common normals of the cutting faces represented in the $\mathbf{S}_a$ coordinate system are the identical to those represented in the $\mathbf{S}_h$ coordinate system, i.e., $\mathbf{n}_a = \mathbf{n}_h$. The velocity of the rack cutter is therefore

$$\mathbf{V}_h^{(F)} = -r_1\omega_1\mathbf{j}_h \tag{35}$$

The velocity of the contact point of the generated cutter is

$$\mathbf{V}_h^{(1)} = \overline{\mathbf{O}_a\mathbf{O}_h} \times \boldsymbol{\omega}_1 + \boldsymbol{\omega}_1 \times \mathbf{r}_a \tag{36}$$

where

$$\overline{\mathbf{O}_a\mathbf{O}_h} = (-r_1 + c)\mathbf{i}_h + r_1\phi_1\mathbf{j}_h \tag{37}$$

The relative velocity is obtained and expressed as

$$\mathbf{V}_h^{(F1)} = \mathbf{V}_h^{(F)} - \mathbf{V}_h^{(1)} \tag{38}$$

(1) The relative velocity between the cutting face I and the generated cutter is as follows:

$$\mathbf{V}_h^{(F1)} = -\omega_1 \left[b_0 - \frac{R}{\tan(45 + \psi_L/2)} - \mathrm{HKW}\tan\psi_L + R\cos\psi_L + \ell^{(I)}\sin\psi_L - r_1\phi_1 \right] \mathbf{i}_h + \omega_1(R - \mathrm{HKW} - R\sin\psi_L + \ell^{(I)}\cos\psi_L - c)\mathbf{j}_h \tag{39}$$

Substituting the common unit normal equation (4) and the relative velocity equation (39) into Eq. (34), the meshing equation becomes:

$$\ell^{(I)} = -(R - \mathrm{HKW} - c)\cos\psi_L - [b_0 - R\cot(45 + \psi_L/2) - \mathrm{HKW}\tan\psi_L - r_1\phi_1]\sin\psi_L \tag{40}$$

Solving this meshing equation (40) and the locus equation (28) simultaneously, the generated tooth profile by cutting face I can thus be obtained.

(2) The relative velocity between the cutting face II and generated cutter is as follows:

$$\mathbf{V}_h^{(F1)} = -\omega_1 \left[\left(-b_0 + \frac{R}{\tan(45 + \psi_R/2)} + \mathrm{HKW}\tan\psi_R - R\cos\psi_R - \ell^{(II)}\sin\psi_R \right) - r_1\phi_1 \right] \mathbf{i}_h + \omega_1(R - \mathrm{HKW} - R\sin\psi_R + \ell^{(II)}\cos\psi_R - c)\mathbf{j}_h \tag{41}$$

Substituting the common unit normal equation (8) and relative velocity equation (41) into Eq. (34), the meshing equation becomes:

$$\ell^{(II)} = (-R + \mathrm{HKW} + c)\cos\psi_R + [-b_0 + R\cot(45 + \psi_R/2) + \mathrm{HKW}\tan\psi_R - r_1\phi_1]\sin\psi_R \tag{42}$$

Solving this meshing equation (42) and the locus equation (29) simultaneously, the generated tooth profile by cutting face II can thus be obtained.

(3) The relative velocity between the cutting face III and the generated cutter is as follows:

$$\mathbf{V}_h^{(F1)} = -\omega_1[b_0 - \frac{R}{\tan(45 + \psi_L/2)} - \mathrm{HKW}\tan\psi_L + R\sin\theta_I - r_1\phi_1]\mathbf{i}_h + \omega_1(R - \mathrm{HKW} - R\cos\theta_I - c)\mathbf{j}_h \tag{43}$$

Substituting the common unit normal equation (12) and the relative velocity equation (43) into Eq. (34), the meshing equation becomes:

$$\theta_I = \tan^{-1}\left\{ \frac{-b_0 + R\cot(45 + \psi_L/2) + \mathrm{HKW}\tan\psi_L + r_1\phi_1}{R - \mathrm{HKW} - c} \right\} \tag{44}$$

Solving this meshing equation (44) and the locus equation (30) simultaneously, the generated tooth profile by cutting face III can thus be obtained.

(4) The relative velocity between the cutting face IV and generated cutter is as follows:

$$\mathbf{V}_h^{(F1)} = -\omega_1 \left[-b_0 + \frac{R}{\tan(45 + \psi_R/2)} + \mathrm{HKW}\tan\psi_R - R\sin\theta_{II} - r_1\phi_1 \right] \mathbf{i}_h + \omega_1(R - \mathrm{HKW} - R\cos\theta_{II} - c)\mathbf{j}_h \tag{45}$$

Substituting the common unit normal equation (16) and relative velocity equation (45) into Eq. (34), the meshing equation becomes:

$$\theta_{II} = \tan^{-1}\left\{ \frac{-b_0 + R\cot(45 + \psi_R/2) + \mathrm{HKW}\tan\psi_R - r_1\phi_1]}{R - \mathrm{HKW} - c} \right\} \tag{46}$$

Solving this meshing equation (46) and the locus equation (31) simultaneously, the generated tooth profile by the cutting face IV can thus be obtained.

(5) The relative velocity between the cutting face V and the generated cutter is as follows:

$$\mathbf{V}_h^{(F1)} = -\omega_1 \left[-b_0 + \frac{R}{\tan(45 + \psi_R/2)} + \mathrm{HKW}\tan\psi_R + \mu - r_1\phi_1 \right] \mathbf{i}_h + \omega_1(-\mathrm{HKW} - c)\mathbf{j}_h \tag{47}$$

Substituting the common unit normal equation (22) and relative velocity equation (47) into Eq. (34), the meshing equation becomes:

$$\mu = \left[b_0 - R\cot\left(45 + \frac{\psi_R}{2}\right) - \mathrm{HKW}\tan\psi_R + r_1\phi_1 \right] \tag{48}$$

Solving this meshing equation (48) and the locus equation (32) simultaneously, the generated tooth profile by cutting face V can thus be obtained.

Table 1 – Parameters of rack cutter and spur-typed cutter

Parameters of shifted spur-typed cutter			
Circular pith (cp, mm)		2.8	
Module (m, mm)		0.89126	
Number of teeth (T)		12	
Height of chamfering (e, mm)		0.3	
Whole depth (HKW + HFW, , mm)		1.77	
Length of cutter (mm)		30	
Pitch diameter (mm)		5.348	
Shifted distance (c, mm)	0.2	0.0	−0.2
Outside diameter (D, mm)	11.791	11.391	10.991
Root diameter (d, mm)	8.251	7.851	7.451
Parameters of rack cutter			
Addendum (HKW, mm)		1.422	
Dedendum (HFW, mm)		0.348	
Tooth thickness ($2b_0$, mm)		1.9	
Tip radius (r, mm)		0.15	
Pressure angle of face I (ψ_L, °)		48	
Pressure angle of face II (ψ_R, °)		3	
Pressure angle of face VI (ψ_3, °)		57	

(6) The relative velocity between the cutting face VI and generated cutter is as follows:

$$\mathbf{V}_h^{(F1)} = -\omega_1[b_0 + (\mathrm{HFW} - e)\tan\psi_L + \ell^{(VI)}\sin\psi_3 - r_1\phi_1]\mathbf{i}_h + \omega_1(\mathrm{HFW} - e + \ell^{(VI)}\cos\psi_3 - c)\mathbf{j}_h \quad (49)$$

The same procedure of substituting the common unit normal equation (26) and relative velocity equation (49) into Eq. (34) gives a meshing equation of

$$\ell^{(VI)} = -(\mathrm{HFW} - e - c)\cos\psi_3 - [b_0 + (\mathrm{HFW} - e)\tan\psi_L - r_1\phi_1]\sin\psi_3 \quad (50)$$

Solving this meshing equation (50) and the locus equation (32) simultaneously, the generated tooth profile by cutting face VI can thus be obtained.

Example 1. A spur-typed cutter has a circular pitch cp = 2.8 mm, with 12 flutes, an outside diameter of 11.391 mm, and a root diameter of 7.851 mm. The relevant parameters are shown in Table 1. The profile of the rack cutter is first designed as shown in Fig. 3. Using the mathematical model developed, the generated spur-typed cutter is shown in Fig. 4. Fig. 4 also shows that the developed mathematical model matches the simulation of the generated rack cutter. The result proves that

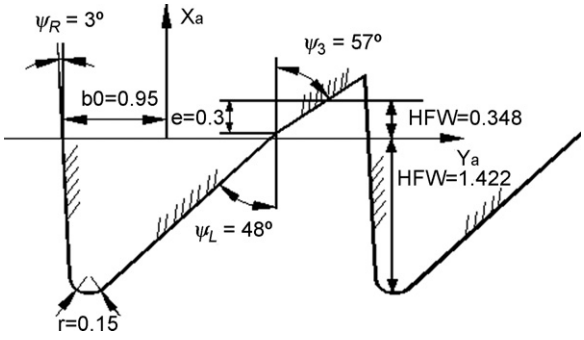

Fig. 3 – Profile of the novel-design rack cutter.

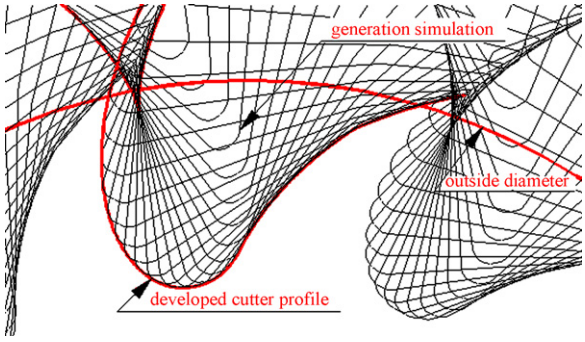

Fig. 4 – Tooth profile and generation simulation of spur-typed cutter ($c = -0.2$).

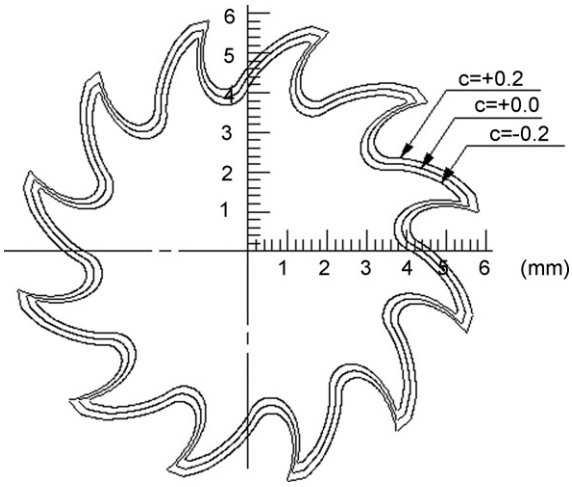

Fig. 5 – Generated tooth profile with different shift amount.

the novel design of using the proposed rack cutter (hob cutter) is an effective and efficient way of manufacturing a spur-typed cutter. Fig. 5 shows the transverse section of the spur-typed cutter. This figure reveals that the same rack cutter with a different shift can produce different spur-typed cutters. Fig. 6 shows the transverse section of a spur-typed cutter with the same outside diameters.

4. Characteristics of the spur-typed cutter

In the preceding section, the mathematical model of the generated spur-typed cutter has been derived. However, the cutting angles and the width of the top land of the cutter will also significantly affect the cutting performance. In this section, these important factors are studied.

4.1. *Full undercutting on the spur-typed cutter*

As previously mentioned, the right cutting face of the proposed spur-typed cutter is generated by undercutting the circular edge of the rack cutter. A poorly designed rack cutter will generate part of an involute curve on a typical cutting edge. When the cutting edge is fully undercut, the starting point of undercutting lies beyond the circle of outside

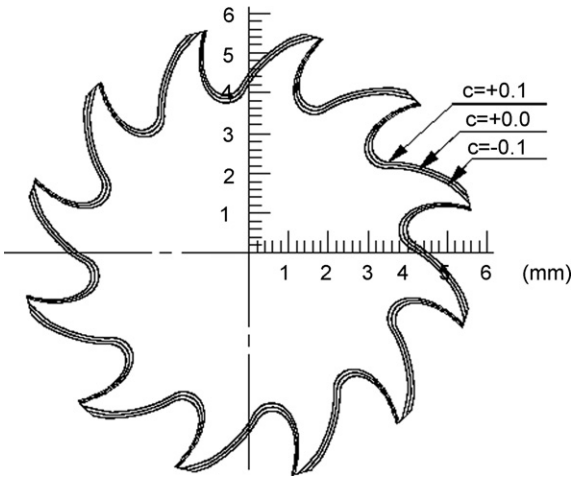

Fig. 6 – Generated tooth profile with different shift amount (outside diameter is constant).

diameter. Hence, the x- and y-components of the equation depicting the right side of the cutting face in Eqs. (29) and (42), respectively, are the same as the x- and y-components of the equation depicting the undercut portion shown in Eqs. (31) and (46).

Example 2. In Example 1, when the shifted distance $c = 0.0$, the radius of the intersection point is $r_P = 5.725$, which is larger than the radius of the outside diameter, $r = 5.696$. This confirms that the design of the rack cutter has satisfied the requirement of a spur-typed cutter.

4.2. *Determination of the cutting angles*

The cutting angles of the end section profile shown in Fig. 7 affect the cutting performance significantly. In this section, the cutting angles of a spur-typed cutter manufactured by the novel hob cutter are investigated. Point A is the intersection point of the undercut portion (region IV) and the curve on the top land of the spur-typed cutter, point B is the intersection point of the chamfered angle edge and the top land curve, and point E is the intersection point of the left cutting edge and the chamfered angle cutting edge. $\mathbf{T}'_A$ and $\mathbf{T}_a$ are the tangential and positional vectors of point A in the $\mathbf{S}_1$ coordinate system, respectively. $\mathbf{T}_B$ is the tangential vector of point B in

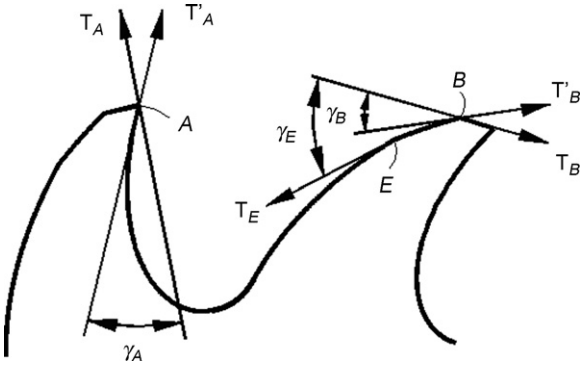

Fig. 7 – Definitions of the cutting angles.

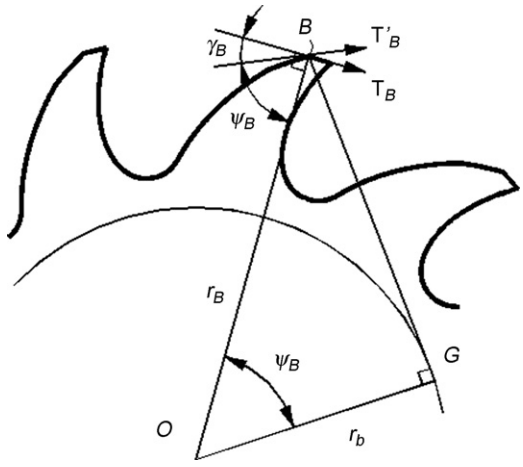

Fig. 8 – The relief angle at point B.

the $\mathbf{S}_1$ coordinate system, and $\mathbf{T}'_B$ is the tangential vector of the chamfered angle cutting edge at point B in the $\mathbf{S}_1$ coordinate system. The radial rake angle γ_A is the angle between $\mathbf{T}_A$ and $\mathbf{T}'_A$, the relief angle γ_B is the angle between $\mathbf{T}_B$ and $\mathbf{T}'_B$, and the clearance angle γ_E is the angle between $\mathbf{T}_B$ and $\mathbf{T}_E$.

4.2.1. *Analysis of the radial rake angle γ_A*

Since point A is the intersection point of the undercut portion (region IV) and the curve on the top land of the spur-typed cutter, the following equation is established:

$$\sqrt{x_A^2 + y_A^2} = r_1 + \mathrm{HFW} \tag{51}$$

where (x_A, y_A) are the coordinates of point A and r_1 is the pitch radius of the spur-typed cutter. Substituting the point A Eqs. (31) and (46) into the above equation, parameter ϕ_1 is obtained. The positional vector $\mathbf{T}_A$ and tangential vector $\mathbf{T}'_A$ of point A can thus be obtained. Vector dot production is then performed to attain γ_A between these two vectors.

4.2.2. *Analysis of the relief angle γ_B*

From the involute curve property (17), the involute curve is extended from the base circle. In Fig. 8, the normal vector of the involute curve at point B is tangent to the base circle. The directional vector $\overrightarrow{OG}$ is thus the same as the tangential vector $\mathbf{T}'_B$ at point B. The pressure angle at point B, i.e., ψ_B is thus obtained as follows:

$$r_B \cos\psi_B = r_b \tag{52}$$

where r_B is the position vector of point B and r_b is the radius of the base circle.

As vectors $\mathbf{T}_B$ and $\mathbf{T}'_B$ are perpendicular to $\overrightarrow{BO}$ and $\overrightarrow{BG}$, respectively, the relief angle γ_B is obtained as

$$\gamma_B = \frac{\pi}{2} - \psi_B \tag{53}$$

4.2.3. *Analysis of the clearance angle γ_E*

In Fig. 9, $\mathbf{T}_E$ is the tangential vector at point E while $\mathbf{T}'_E$ is the vector perpendicular to the position vector $\mathbf{r}_E$. Applying the theory of involutometry, the clearance angle γ_E is obtained as

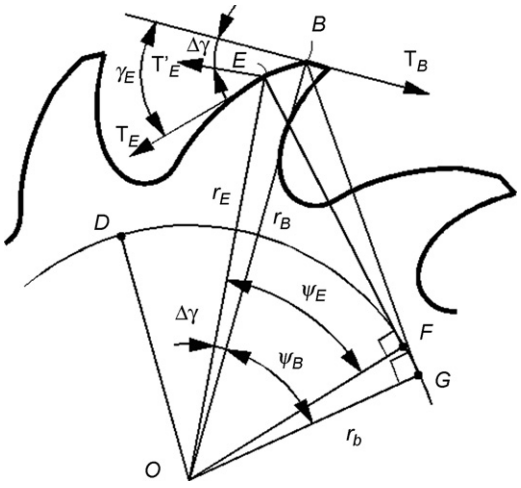

Fig. 9 – Relationship between clearance angles γ_E and $\Delta\gamma$ at point E.

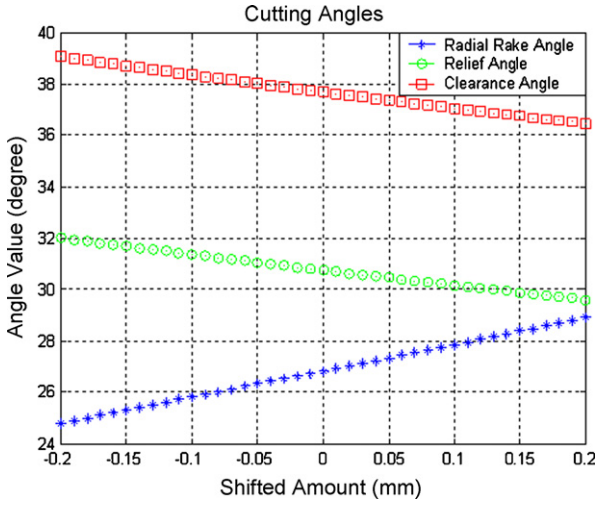

Fig. 10 – The cutting angles when outside diameters are changed according to the shifted amount.

follows:

$$\gamma_E = \frac{\pi}{2} + \Delta\gamma - \psi_E \tag{54}$$

where

$$\Delta\gamma = \text{inv}\,\psi_B - \text{inv}\,\psi_E \tag{55}$$

4.2.4. *Effect of shifted distance on the cutting angles*

By substituting the values from Table 1, the various cutting angles are obtained and shown in Fig. 10 where the outside diameters are changed according to the shifted distance. If the outside diameters are kept constant, the cutting angles are as shown in Fig. 11.

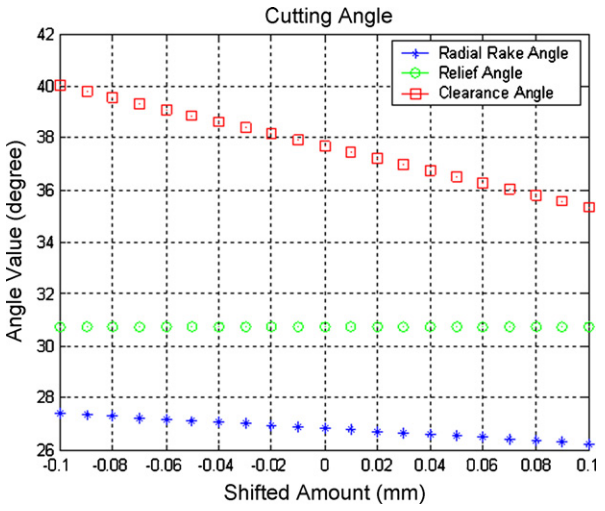

Fig. 11 – The cutting angles when the outside diameters are kept constant.

4.3. *Width of top land of spur-typed cutter*

The width of the top land of the spur-typed cutter can be obtained by solving for the coordinates of points A and B shown in Fig. 12. The coordinates of point A were solved in the previous section. If the polar angle η of point B is solved, the x-component of point B is $B_x = r_B \cos\eta$ and the y-component is $B_y = r_B \sin\eta$. From the geometric relationship shown in Fig. 12, η can be expressed as

$$\eta = \angle\text{KOE} + \angle\text{EOB} \tag{56}$$

where

$$\angle\text{EOB} = \text{inv}\,\psi_B - \text{inv}\,\psi_E \tag{57}$$

Due to pure rolling between the pitch line of the rack cutter and the pitch circles of the generated gears, the arc length of NJ shown in Fig. 12 is equal to the corresponding distance ℓ

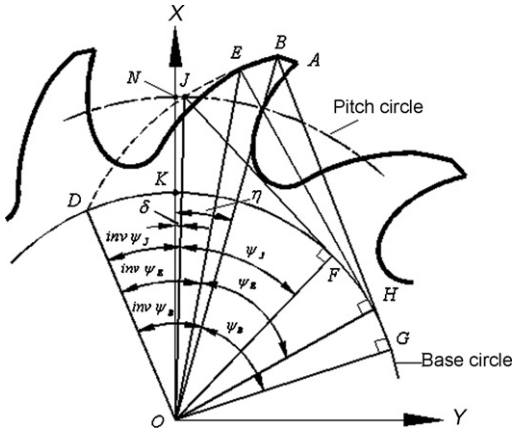

Fig. 12 – Pressure angles at different points.

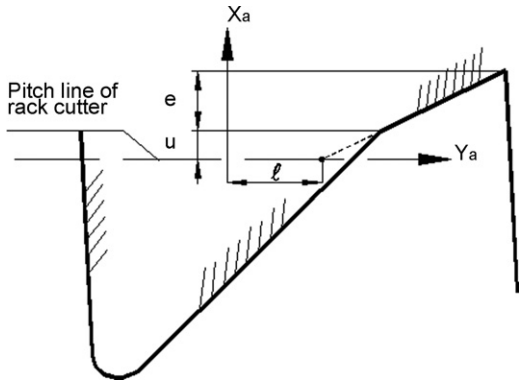

Fig. 13 – Rolling position of the largest pressure angle for the rack cutter.

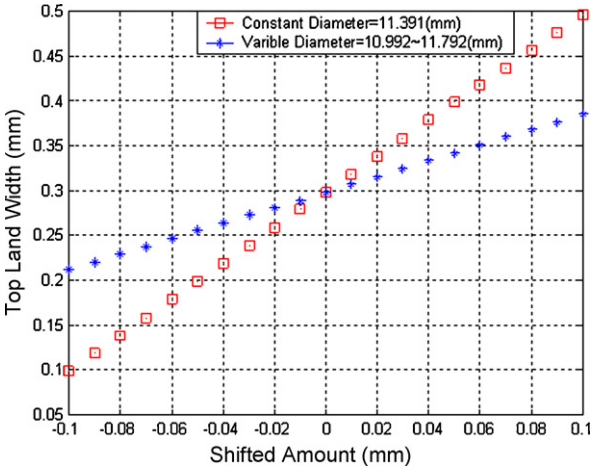

Fig. 14 – Width of top land of spur-typed cutter with constant outside diameter, and variable outside diameter according to the shifted amount, respectively.

shown in Fig. 13. The angle $\delta = \angle NOJ$ is therefore

$$\delta = \frac{\ell}{r_1} \tag{58}$$

where r_1 is the radius of the pitch circle of the generated spur-typed cutter.

Therefore, angle η is obtained as

$$\eta = \text{inv}\,\psi_B - \text{inv}\,\psi_J + \delta \tag{59}$$

Fig. 14 shows the width of the top land of the spur-typed cutter when the outside diameters are kept constant, and when the outside diameters are changed according to the shifted distance, respectively.

5. Conclusion

A novel design for a hob cutter capable of generating a spur-typed cutter in one hobbing process has been proposed. The cutting edge in the normal direction has been designed as three straight lines with different pressure angles and two arcs. By applying the equations of the rack profiles of the cutting edges, the principle of coordinate transformation, the theory of differential geometry, and the theory of gearing, the mathematical models of the spur-typed cutter profile, including the radial cutting angle, relief angle, and clearance angle have been derived. A computer simulation involving a parametric study of the three angles was also carried out. The major characteristics of the generated spur-typed cutter were also studied in this paper. The proposed method can be used as design guidance in designing novel hob-type cutters to generate spur-typed cutters. Moreover, it is expected that the results from this paper will contribute to the improvement of the manufacture of plain mill cutters and provide the tool industry with a reference for designing and machining similar tools. The results can also act as a basis for researchers to optimise and improve their tool designs.

Acknowledgments

The work outlined in this paper was supported by the national science council under grants NSC91-2212-E-150-022 and NSC92-2212-E-150-033.

REFERENCES

Ainoura, M., Nagano, K., 1987. The effect of reverse hobbing at a high speed. Gear Technol. 4 (March/April (2)), 8–15.
Bouzakis, K.D., Antonidais, A., 1995. Optimizing of tangential tool shift in gear hobbing. Ann. CIRP 44 (1), 75–78.
Chang, S.L., 1996. Gear hobbing simulation of CNC gear hobbing machines. Dissertation for Doctoral Degree. National Chaio Tung University, Hsinchu, Taiwan, ROC.
Chang, S.L., Liu, J.Y., Hsieh, L.C., 2002. Design of hob cutters for generating helical cutting tools with multi-cutting angles. Chinese Patent 185894.
Chang, S.L., Tsay, C.B., Nagata, S., 1997a. A general mathematical model for gear generated by CNC hobbing machine. Trans. ASME J. Mech. Design 119, 108–113.
Chang, S.L., Tsay, C.B., Tseng, C.H., 1997b. Kinematic optimization of a modified helical simple gear train. Trans. ASME J. Mech. Design 119, 307–314.
Chang, S.L., Tsay, C.B., Wu, L.I., 1996. Mathematical model and undercutting analysis of elliptical gears generated by rack cutters. Mech. Mach. Theory 31 (7), 879–890.
Cluff, B.W., 1987. Effects of hob quality and resharpening errors on generating accuracy. Gear Technol. 4 (September/October (5)), 37–46.
Kapelevich, A., 2000. Geometry and design of involute spur gears with asymmetric teeth. Mech. Mach. Theory 35, 117–130.
Koelsch, J.R., 1994. Hobs in high gear. Manuf. Eng. (July), 67–69.
Liu, J.Y., Chang, S.L., 2003. Design of hob cutters for generating helical cutting tools with multi-cutting angles. Int. J. Mach. Tools Manuf. 43 (12), 1185–1195.
Litvin, F.L., 1989. Theory of Gearing. NASA Publication, Washington, DC.
Phillips, R., 1994. New innovations in hobbing. Part I. Gear Technol. 11 (September/October (5)), 16–20.
Radhakrishnan, T., Kawlra, R.K., Wu, S.M., 1982. A mathematical model of the grinding wheel profile required for a specific twist drill flute. Int. J. Mach. Tool Design Res. 22, 239–251.
Tsay, C.B., 1988. Helical gears with involute shaped teeth: geometry, computer simulation, tooth contact analysis, and stress analysis. Trans. ASME J. Mech. Transm. Autom. Design 110, 482–491.